Temperature Fiber Sensors Based on Mach–Zehnder Interferometer With Sturdy Structure

Jui-Ming Hsu, Wen-Hao Zheng, Jian-Zhi Chen, Cheng-Ling Lee, *Member, IEEE*, and Jing-Shyang Horng

***Abstract*— This paper presents a highly sensitive and in-line temperature fiber sensor based on Mach–Zehnder interferometer with material overlay. The sensor is constructed using a section of single-mode fiber sandwiched between a no-core fiber and a waist-enlarged taper and immersed in a material with high thermo-optic coefficient. The experimental results indicated that a high temperature sensitivity of 0.825 nm/°C was accomplished for surrounding material with the refractive index of ∼1.45. The proposed sensor has numerous merits of in-line applications, high sensitivity, easy fabrication, simple structure, compact size, and furthermore, the structure is sturdy due to its high mechanical strength.**

***Index Terms*— Fiber taper, interferometers, Mach-Zehnder interferometers, optical fiber sensors, temperature sensors.**

I. Introduction

OPTICAL fiber sensors have many advantages, such as small size, fast response, corrosion resistance, and immunity to electromagnetic interference, so have been well developed and studied in various sensing application such as refractive index (RI) [1]–[4], temperature [5]–[9], strain [4], displacement [10], curvature [11], humidity [12], liquid level [13], directional tilt [14], etc.

Numerous structures of optical fiber sensors have been proposed using various techniques, the all-fiber Mach-Zehnder interferometers (MZI) have been intensively studied, due to their advantages such as no couplers required, high sensitivity, applicability for remote sensing and ease of fabrication. In terms of temperature measurement many types of MZI have been constructed including liquid-sealed S fiber taper [5], adding a taper to a single mode-multimode-single mode fiber (SMS) [6], photonic crystal fiber [7], fs-laser make inner air cavity [9], using S fiber taper in fiber bragg grating [15]. However, these sensors have some disadvantages of fragile structure, complicated fabrication, or expensive cost, etc.

Waist-enlarged taper (WET) have attracted substantial attention recently due to their advantages such as easy fabrication, tough structure. Many structures of sensors with WET have been proposed, such as concatenated taper and WET for RI sensing applications [2], multimode fiber core sandwiched between two WETs [3], two peanut-shape structures [16].

Manuscript received April 25, 2015; revised August 10, 2015; accepted August 12, 2015. Date of publication August 19, 2015; date of current version October 8, 2015. The associate editor coordinating the review of this paper and approving it for publication was Dr. Anna G. Mignani. *(Corresponding author: Jui-Ming Hsu.)*

The authors are with the Department of Electro-Optical Engineering, National United University, Miaoli 360, Taiwan (e-mail: juiminghsu@gmail.com; taiwanandme@hotmail.com.tw; supercliff301@gmail.com; cherry@nuu.edu.tw; jshorng@nuu.edu.tw).

Color versions of one or more of the figures in this paper are available online at http://ieeexplore.ieee.org.

Digital Object Identifier 10.1109/JSEN.2015.2469670

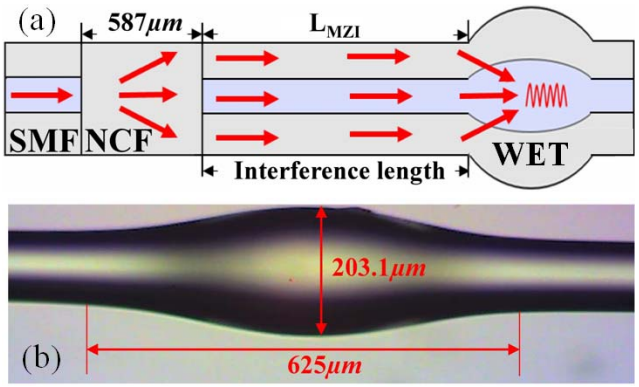

Fig. 1. (a) Configuration of the proposed MZI. (b) Microscope photograph of the WET.

Fiber-based temperature sensors typically have a low temperature sensitivity because silica fiber has an extremely low thermal expansion coefficient (TEC=$+5.5\times10^{-7}$ °C^{-1}) and thermo-optic coefficient (TOC=$+5\times10^{-6}$ °C^{-1}). In this paper, we present a temperature sensor based on MZI, surrounding the sensor with a high TOC material (TOC= -3.74×10^{-4} °C^{-1}) for enhancing sensitivity. The sensor is constructed by using a piece of single mode fiber (SMF) sandwiched between a no-core fiber (NCF) and a WET. The structure has higher mechanical strength than an ordinary taper structure. For surrounding oil with a RI of 1.45, the temperature sensitivities are 0.825 nm/°C and 0.240 nm/°C in the range of 20 °C to 30 °C and 30 °C to 60 °C, respectively.

In order to easily construct a sturdy sensor, this work first adopted two simple and rigid elements, NCF and WET, as the components of the sensor. In a word, the sensor has merits of in-line applications, high sensitivity, easy fabrication, simple structure, compact size, and sturdy structure.

II. Configuration and Principles

Figure 1(a) presents the configuration of the proposed MZI sensor. A section of SMF (called interference SMF in this paper) with a length of L_{MZI}, which is so-called interference length, is sandwiched between a NCF and a WET. A light beam from the lead-in SMF is split into the core and cladding modes at the interface between the lead-in SMF and NCF, the core and cladding modes propagate through the NCF, and inject into the interference SMF. By the WET, some cladding

1530-437X © 2015 IEEE. Personal use is permitted, but republication/redistribution requires IEEE permission.
See http://www.ieee.org/publications_standards/publications/rights/index.html for more information.

modes are coupled into the core, and unite with the core mode. Finally, the united beam outputs through a lead-out SMF.

As the core and cladding modes pass through the interference SMF, phase differences between the core and cladding modes are introduced, thus the united beam brings about interference and propagates to the output. The optical phase difference between the core and m-th order cladding mode after propagating through the length L_{MZI} of the interference SMF can be written as

$$\phi_m = \frac{2\pi}{\lambda}(n_{eff}^{co} - n_{eff}^{cl,m})L_{MZI} = \frac{2\pi}{\lambda}\Delta n_{eff}^{m} L_{MZI}, \quad (1)$$

where λ represents wavelength, n_{eff}^{co} and $n_{eff}^{cl,m}$ are the effective indices of the fundamental core mode and the coupling cladding mode of m-th order, respectively.

The length (L_{NCF}) and diameter of the NCF are 587 μm and 125 μm, respectively. Figure 1(b) shows the microscope photograph of the WET, the length and the diameter at waist are about 625.0 μm and 203.1 μm, respectively. For fabricating the WET, an electrical arc method was employed by using Ericsson FSU-975 commercial fusion splicer. A user-defined fiber taper program revised from the original "SMF taper program" of the fusion splicer was created firstly. The specific fabrication process can be found in [17]. The prefusion time and prefusion current are kept in default. The parameters of the overlap, the discharge current and the fusion time are set as 49.9 μm, 14 mA, and 6 sec, respectively, for fusion splicing. After heating by the prefusion process, the fiber is softened. The SMF was then compressed simultaneously when the arc was discharging, thus the WET shown in Fig. 1(b) was formed. The parameters set for each splicing are identical; this will result in a same geometrical shape of the WETs. On the other hand, the NCF can be cut using a high precision cleaver. Therefore, the reproducibility of the proposed sensor could be ensured.

In this work, the L_{NCF} was pre-estimated by using the beam propagation method (BPM). As shown in Fig. 2(a), the simulated fiber combines a section of lead-in SMF and NCF with lengths of 100 μm and 900 μm, respectively. A light beam from the lead-in SMF spreads out in the NCF and forms self-imaging [18] at periodic intervals along the NCF. The field pattern at the distance of 1000 μm (L_{NCF}=900 μm), which is displaced in Fig. 2(b), declares a fact that the core mode from the lead-in SMF is almost vanished due to the effect of multimode interference (MMI). On the contrary, for a short propagation distance of 300 μm (L_{NCF}=200 μm) as shown in Fig. 2(d), the spread of the field is not enough to result abundant cladding modes. According to interference principle, to achieve a high extinction ratio modal interference, the intensities of the two interference modes must be nearly identical. The cases of Fig. 2(b) and 2(d) violate this principle. The field pattern of L_{NCF}=500 μm shown in Fig. 2(c) indicates a happy medium for interference. The appropriate L_{NCF} is about 500 μm~600 μm in our experience. For shorter L_{NCF}, the intensity of the core mode is much higher than that of cladding mode. For larger L_{NCF}, the MMI effect governs the intensity distinction between the core and cladding modes. This brings about an uncertain situation.

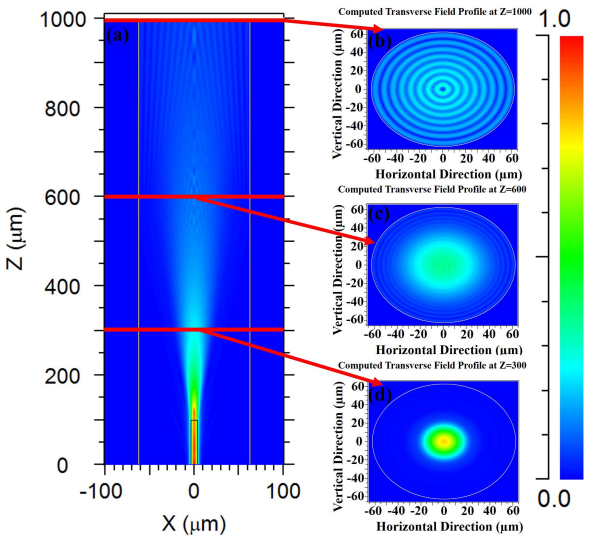

Fig. 2. (a) Simulated field propagates in a combination of lead-in SMF (Z=0~100 μm) and NCF (Z=100~1000 μm), and cross-sectional views of the field patterns at the distances of (b) 1000 μm, (c) 600 μm, and (d) 300 μm.

The light spread in the NCF is then injected into the interference SMF. The fields of the light propagated in the interference SMF were simulated by using the BPM again, and the results are shown in Fig. 3. The simulated fiber in the figure is composed by sandwiching a section of NCF between the lead-in SMF and the interference SMF, the lengths of lead-in SMF, NCF, and interference SMF are 100 μm, 587 μm, and 1.2 cm, respectively. Figure 3(a)-(d) display the fields propagate in the fiber surrounded by the material with RI (n_D) of 1.33 (Fig. 3(a)), 1.39 (Fig. 3(b)), 1.44 (Fig. 3(c)), and 1.45 (Fig. 3(d)), respectively. Figure 3(e)-(h) demonstrate the cross-sectional views of the field patterns at the distances of Z=1310 μm for the surrounding materials with n_D=1.33 (Fig. 3(e)), 1.39 (Fig. 3(f)), 1.44 (Fig. 3(g)), and 1.45 (Fig. 3(h)), respectively. The contour levels shown in the inset represent the powers normalized with lunched into the lead-in SMF. As shown in the figures, as expectancy, abundant cladding modes are produced in the cladding for each surrounding materials, this can be ascribed to the appropriate length of NCF. Furthermore, for n_D=1.44 and 1.45, the cladding modes stretch out their mode field into the surrounding due to the RI of the surrounding approximates to that of the cladding. This phenomenon is especially severe for the case of n_D=1.45.

Figure 4 indicates the experimental setup of the proposed MZI sensor. Light from a wide band light source (WBLS) with a wavelength range of 1250-1650 nm is launched into the MZI, and transmission spectra are detected by an optical spectrum analyzer (OSA). The MZI is laid on a U-groove, which is used to contain the surrounding liquid, the Cargille index oil with a high TOC of -3.74×10^{-4} °C^{-1}, and fixed two ends by fixed stages to avoid the influence of bending interference. The applied temperature T(°C) is controlled by a TE cooler from 20 °C to 60 °C to measure the spectral variation with T-changing.

Figure 5 shows the transmission spectra of the MZI structures without material overlay, i.e. in air, in room temperature.

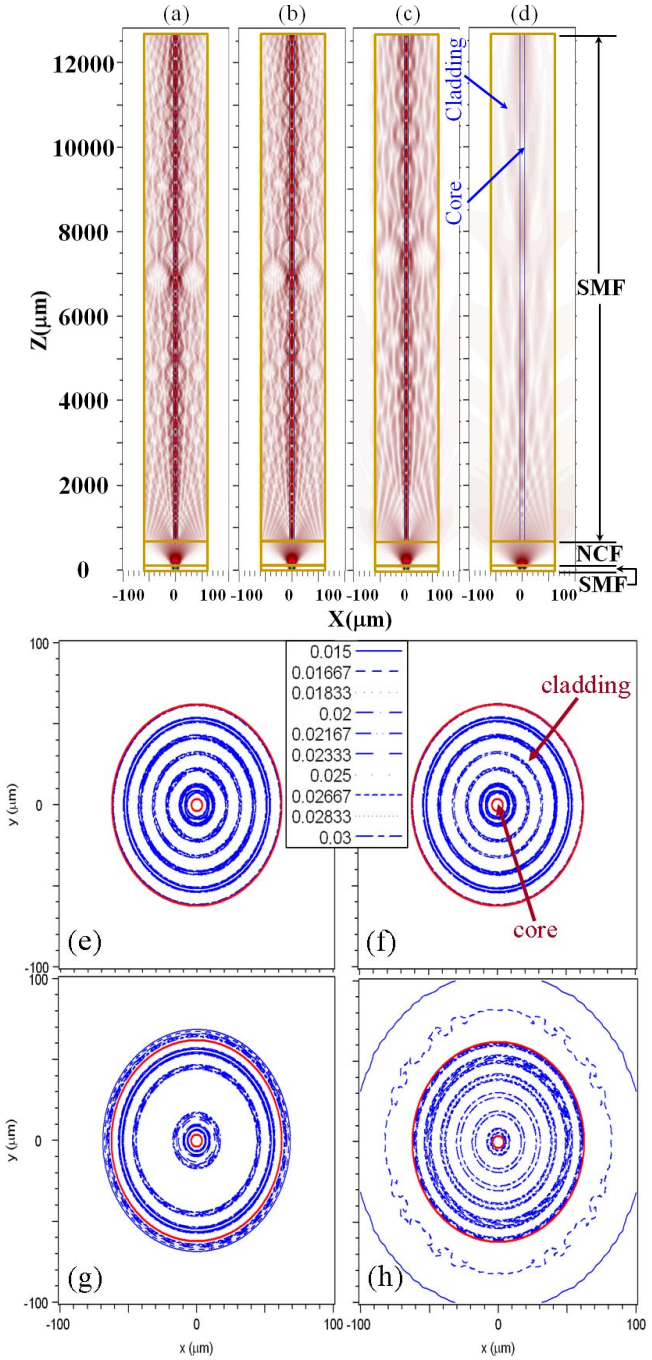

Fig. 3. Simulated field propagated in a combination of SMF-NCF-SMF immersed in the material with the n_D of (a) 1.33, (b) 1.39, (c) 1.44, (d) 1.45, and cross-sectional views of the field patterns at the distances of Z=1310 μm for the surrounding with the n_D of (e) 1.33, (f) 1.39, (g) 1.44, (h) 1.45. The contour levels in the inset represent the normalized powers.

As shown in the figure, the loss is about 10 dB for the three cases due to beam-split in the NCF. The structure without WET reveals no interference because the cladding modes can't couple into the core without WET, and can't interfere with the core mode. For the structures with WET (two cases of L_{MZI}=1 cm and 1.2 cm), a cladding mode and the core mode are assembled at the WET and result interference.

The wavelength of spectral minima $\lambda^m_{\min}$ can be deduced by substituting the condition of interference minima

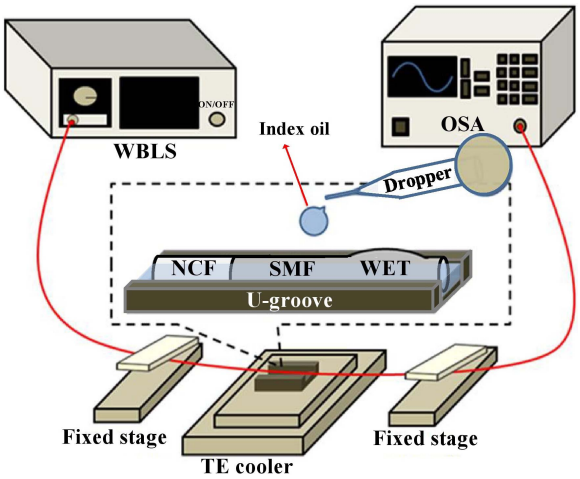

Fig. 4. Experimental setup for measuring the temperature by the proposed MZI sensor.

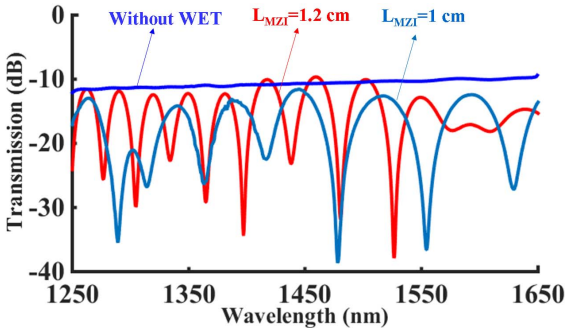

Fig. 5. Transmission spectra of the MZI structures without material overlay (in air) in room temperature.

$\phi_m=(2n+1)\pi$, where n is an integer, into Eq. (1):

$$\lambda^m_{\min} = \frac{2}{2n+1}\Delta n^m_{eff} L_{MZI}. \tag{2}$$

In addition, from Eq. (1), the free space range (*FSR*), the wavelength separation between two interference minima, can be approximated as:

$$FSR \approx \frac{\lambda^2}{\Delta n^m_{eff} L_{MZI}}. \tag{3}$$

As shown in Fig. 5, a larger L_{MZI} results in a smaller *FSR*, this can be clarified by Eq. (3).

III. Experimental Results and Discussion

Figure 6 shows the experimental spectra of the proposed MZI temperature sensor with L_{MZI}=1.2 cm overlaid with materials of various RI values. At lower surrounding RI, the MZI has a very poor sensitivity to external temperature. Owing to the greater parts of cladding modes are confined in the cladding, as shown in Fig. 3, which is formed with pure silica with an extremely low TOC. Therefore, the variations in Δn^m_{eff} with temperature are smaller. The MZI immersed in a surrounding with the *RI* of n_D=1.45 is most sensitive to temperature. This occurs because, at n_D=1.45, the cladding

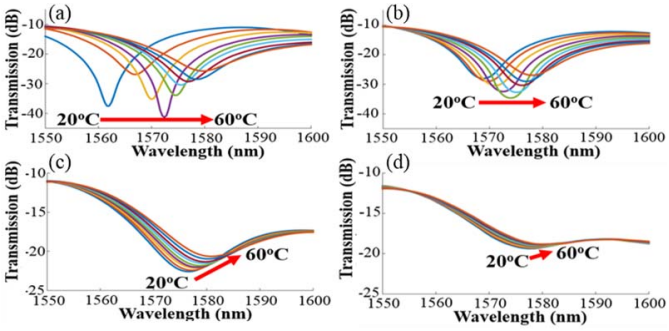

Fig. 6. Experimental transmission spectra of the proposed MZI temperature sensor with various T for material surroundings with indices of (a) n_D=1.45, (b) n_D=1.44, (c) n_D=1.39, and (d) n_D = 1.33. L_{NCF}=587 μm, L_{MZI}=1.2 cm.

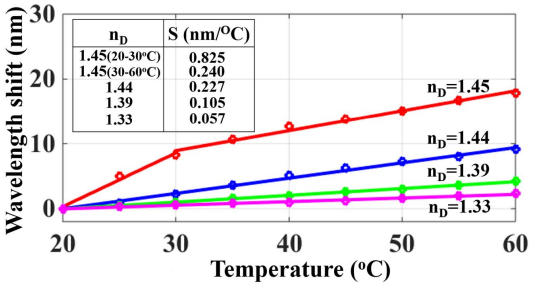

Fig. 7. Sensitivities of shifts in wavelengths of MZIs with surroundings of various *RI* values. Inset shows the corresponding sensitivity of the used index oil. L_{NCF}=587 μm, L_{MZI}=1.2 cm.

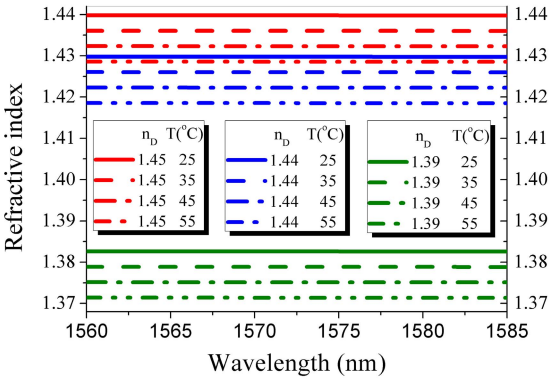

Fig. 8. Relationship between the RIs of the surrounding materials and wavelengths at various temperatures for the proposed MZI. L_{NCF}=587 μm, L_{MZI}=1.2 cm.

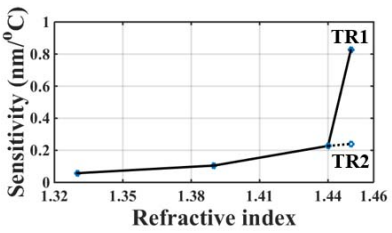

Fig. 9. Dependence of temperature sensitivity on the RI of surrounding material. L_{NCF}=587 μm, L_{MZI}=1.2 cm. (for n_D=1.45, TR1: T=20-30°C; TR2: T=30-60°C.)

modes greatly stretch out their mode fields into the surrounding which has a high TOC, as shown in Fig. 3, thus the Δn_{eff}^m is influenced by the surrounding severely.

As shown in the figures, the spectra move to longer wavelength with temperature increasing. This phenomenon can be explained as follows: as temperature increase, the environmental refractive index decreases due to the negative TOC of the surrounding, thus the effective index of the cladding modes may decrease and that of the core mode does not change much, and Δn_{eff}^m will increase accordingly. Consequently, the spectra should shift to longer wavelength according to Eq. (2).

Figure 7 shows the fitted linear response of the sensitivities for various *RI*s of the material and the inset lists the relation between n_D and sensitivity in nm/°C. Here, the n_D values of the used Cargille index oil are measured at 25°C, Sodium D Line, and λ = 589.3 nm. The results reveal a highly linear response to temperature. Furthermore, the sensor has high sensitivity when the *RI* of the surrounding material approaches that of the fiber (n_D=1.45). Because the cladding modes, as mentioned above, strongly stretch out into the surroundings with a TOC much higher than silica, thus the Δn_{eff}^m varies with great sensitivity for T-changing. Figure 7 appears saturation of sensitivity response for n_D=1.45 in the temperature range of T>30°C, this can be explained as follows. The surrounding material drops its RI for higher temperature, and the lower RI causes the cladding modes shrink their mode fields back to the fiber and induces lower sensitivity as mentioned above. Therefore, higher temperature reduces the sensitivity for the case of n_D=1.45. By respectively using the Cauchy equations and TOC of the Cargille index oils of n_D=1.45, 1.44 and 1.39, the relationship between the RIs, at the temperatures of 25, 35, 45, and 55°C, of the surrounding materials and wavelengths for the proposed MZI is shown in Fig. 8. The Cauchy equation is given by

$$RI(\lambda) = A + \frac{B}{\lambda^2} + \frac{C}{\lambda^4} \tag{4}$$

where λ is the vacuum wavelength in angstroms, A, B, and C are the Cauchy coefficients which vary with different materials. As shown in the figure, the refractive indices of the surrounding materials appear slightly downward sloping curves toward longer wavelength due to Eq. (4) and obviously decrease with temperature increasing caused by the negative TOC. It is obvious, for a higher temperature, the RIs of n_D=1.45 drop into the "RI range" of n_D=1.44. Therefore, as shown in the inset of Fig. 7, the sensitivity for n_D=1.45 at higher temperatures approaches to that of n_D=1.44.

Figure 9 demonstrates the dependence of temperature sensitivity on the RI of surrounding material. In the figure, for n_D=1.45, TR1 and TR2 represent different temperature range of 20 °C to 30 °C, and 30 °C to 60 °C, respectively. Comparing the temperature sensitivity for various surrounding RI values (n_D), TR1 of n_D=1.45 exhibits an extremely high sensitivity (S=0.825 nm/°C). Comparatively, TR2 of n_D=1.45 reveals a lower sensitivity (S=0.240 nm/°C) due to the saturation condition mentioned above. Even so, the sensitivities of the proposed sensor with n_D=1.45 are much higher than the previous works. For the surrounding materials

TABLE I
PROPOSED SENSOR IS COMPARED IN TERMS OF SENSITIVITY AND TEMPERATURE RANGE WITH OTHER FIBER OPTIC TEMPERATURE SENSORS

Ref.	Structure (Type)	Sensitivity (pm/°c)	Temperature range
The work	NCF-SMF-WET with Material Overlay (MZI)	825 240	20 ℃ to 30 ℃ 30 ℃ to 60 ℃
[5]	Liquid-Sealed S-Taper (MZI)	-1403	20 ℃ to 50 ℃
[6]	MMF-SMF-Taper (MZI)	85.8 128.6	100 ℃ to 400 ℃ 400 ℃ to 850 ℃
[7]	PCF with Material Overlay (MZI)	-920	25 ℃ to 50 ℃
[8]	Liquid filled PCF (MI)	5400	25 ℃ to 30 ℃
[9]	Air cavity in SMF (MZI)	43.2	27 ℃ to 1000 ℃
[15]	S-Taper in FBG (MZI&FBG)	14.71	28 ℃ to 95 ℃

* MZI: Mach-Zehnder interferometer
MI: Michelson interferometer
FBG: Fiber Bragg Grating

with n_D<1.45, the temperature sensitivities are even lower than the cases of TR1 and TR2 of n_D=1.45.

Table I shows comparisons for the sensitivities and temperature ranges of the proposed sensor with other fiber optic temperature sensors. In overview, using a high TOC material in the device can enhance the sensitivity of the sensor; nevertheless, that will reduce the wavelength range in use. The using of taper or S-taper is fragile, that of PCF is more expensive, and some structures are complicated in fabrication. The proposed sensor has advantages of high sensitivity, easy fabrication, simple structure, and sturdy structure as mentioned above. Every sensor has its strong and weak points, one can select a suitable structure depend on the application.

IV. CONCLUSION

A simple in-line temperature fiber sensor based on MZI with high sensitivity is proposed. Immersing the proposed NCF-SMF-WET structure in a high TOC material with a RI of 1.45 had demonstrated that high temperature sensitivities of 0.825 nm/°C (20-30 °C) and 0.240 nm/°C (30-60 °C) were accomplished. The sensor has merits of in-line applications, high sensitivity, easy fabrication, simple structure, compact size, and furthermore the structure is sturdy due to its high mechanical strength.

REFERENCES

[1] F. Shi, J. Wang, Y. Zhang, Y. Xia, and L. Zhao, "Refractive index sensor based on S-tapered photonic crystal fiber," *IEEE Photon. Technol. Lett.*, vol. 25, no. 4, pp. 344–347, Feb. 15, 2013.

[2] S. Zhang, W. Zhang, P. Geng, and S. Gao, "Fiber Mach–Zehnder interferometer based on concatenated down- and up-tapers for refractive index sensing applications," *Opt. Commun.*, vol. 288, pp. 47–51, Feb. 2013.

[3] M. Shao, X. Qiao, H. Fu, Y. Liu, X. Zhao, and N. Yao, "High sensitivity refractive index sensing of Mach–Zehnder interferometer based on multimode fiber core sandwiched between two waist-enlarged fiber tapers," *Opt. Commun.*, vol. 311, pp. 359–363, Jan. 2013.

[4] R. Yang *et al.*, "S-tapered fiber sensors for highly sensitive measurement of refractive index and axial strain," *J. Lightw. Technol.*, vol. 30, no. 19, pp. 3126–3132, Oct. 1, 2012.

[5] R. Yang *et al.*, "A highly sensitive temperature sensor based on a liquid-sealed S-tapered fiber," *IEEE Photon. Technol. Lett.*, vol. 25, no. 9, pp. 829–832, May 1, 2013.

[6] Y. Liu, W. Peng, Y. Liang, X. Zhang, X. Zhou, and L. Pan, "Fiber-optic Mach–Zehnder interferometric sensor for high-sensitivity high temperature measurement," *Opt. Commun.*, vol. 300, pp. 194–198, Jul. 2013.

[7] J.-M. Hsu, C.-L. Lee, P.-J. Huang, C.-H. Hung, and P.-Y. Tai, "Temperature sensor with enhanced sensitivity based on photonic crystal fiber interferometer with material overlay," *IEEE Photon. Technol. Lett.*, vol. 24, no. 19, pp. 1761–1764, Oct. 1, 2012.

[8] J.-M. Hsu, J.-S. Horng, C.-L. Hsu, and C.-L. Lee, "Fiber-optic Michelson interferometer with high sensitivity based on a liquid-filled photonic crystal fiber," *Opt. Commun.*, vol. 331, pp. 348–352, Nov. 2014.

[9] T. Y. Hu, Y. Wang, C. R. Liao, and D. N. Wang, "Miniaturized fiber in-line Mach–Zehnder interferometer based on inner air cavity for high-temperature sensing," *Opt. Lett.*, vol. 37, no. 24, pp. 5082–5084, 2012.

[10] C.-Y. Shen *et al.*, "High sensitive micro-displacement sensor based on M-Z interferometer by a bowknot type taper," *IEEE Photon. Technol. Lett.*, vol. 26, no. 1, pp. 62–65, Jan. 1, 2014.

[11] S. Zhang, W. Zhang, S. Gao, P. Geng, and X. Xue, "Fiber-optic bending vector sensor based on Mach–Zehnder interferometer exploiting lateral-offset and up-taper," *Opt. Lett.*, vol. 37, no. 21, pp. 4480–4482, 2012.

[12] L. H. Chen *et al.*, "Chitosan based fiber-optic Fabry–Perot humidity sensor," *Sens. Actuators B, Chem.*, vol. 169, pp. 167–172, Jul. 2012.

[13] J.-M. Hsu, C.-L. Lee, H.-P. Chang, W. C. Shih, and C.-M. Li, "Highly sensitive tapered fiber Mach–Zehnder interferometer for liquid level sensing," *IEEE Photon. Technol. Lett.*, vol. 25, no. 14, pp. 1354–1357, Jul. 15, 2013.

[14] C.-L. Lee, W.-C. Shih, J.-M. Hsu, and J.-S. Horng, "Asymmetrical dual tapered fiber Mach–Zehnder interferometer for fiber-optic directional tilt sensor," *Opt. Exp.*, vol. 22, no. 20, pp. 24646–24654, 2014.

[15] J. Li *et al.*, "Simultaneous force and temperature measurement using S fiber taper in fiber Bragg grating," *IEEE Photon. Technol. Lett.*, vol. 26, no. 3, pp. 309–312, Feb. 1, 2014.

[16] D. Wu, T. Zhu, K. S. Chiang, and M. Deng, "All single-mode fiber Mach–Zehnder interferometer based on two peanut-shape structures," *J. Lightw. Technol.*, vol. 30, no. 5, pp. 805–810, Mar. 1, 2012.

[17] X. Wen *et al.*, "Dumbbell-shaped Mach–Zehnder interferometer with high sensitivity of refractive index," *IEEE Photon. Technol. Lett.*, vol. 25, no. 18, pp. 1839–1842, Sep. 15, 2013.

[18] L. B. Soldano and E. C. M. Pennings, "Optical multi-mode interference devices based on self-imaging: Principles and applications," *J. Lightw. Technol.*, vol. 13, no. 4, pp. 615–627, Apr. 1995.

Jui-Ming Hsu received the Ph.D. degree in optical science from the Institute of Optical Science, National Central University, Chung-Li, Taiwan, in 1998. He has been with the Chung Shan Institute of Science and Technology since 1980, and the Department of Electro-Optical Engineering, National United University, Maioli, Taiwan, as an Assistant Professor, since 2006, and was promoted to Associate Professor in 2013. His current research interests include fiber sensors, photonic crystal devices, and fibers.

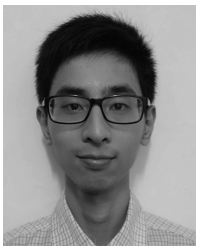

Wen-Hao Zheng was born in Hsinchu, Taiwan, in 1991. He received the B.S. degree from the Department of Electro-Optical Engineering, National United University, Taiwan, in 2009, and the M.S. degree from the Institute of Electro-Optical Engineering, National United University, in 2015. His research interests include fiber based devices and optical fiber sensors.

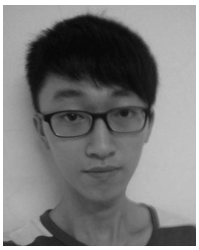

Jian-Zhi Chen was born in Yunlin, Taiwan, in 1993. He is currently pursuing the bachelor's degree with the Department of Electro-Optical Engineering, National United University, Miaoli, Taiwan. His current research interests are in the field of optical fiber sensing and electro-optical technology.

Cheng-Ling Lee (M'10) received the Ph.D. degree from the Institute of Electro-Optical Engineering, National Chiao Tung University, Hsinchu, Taiwan, in 2003. From 2004 to 2010, she was an Associate Professor with the Department of Electro-Optical Engineering, National United University, Miaoli, Taiwan. In 2011, she became a Full Professor. She is a member of OSA Optical Society. She has authored over 40 peer-reviewed publications in scientific journals. Her special fields of interests include fiber-based devices, optical fiber sensors, and fiber gratings synthesis.

Jing-Shyang Horng received the Ph.D. degree from the Institute of Electronics, National Chiao Tung University, Taiwan, in 1988. From 1988 to 1996, he was an Engineer with the Electro-Optical System Laboratory, Institute of Industrial Technology Research, Hsinchu, Taiwan. He is currently an Associate Professor with the Department of Electro-Optical Engineering, National United University, Taiwan. His special fields of interest include classical diffraction optics, packaging of laser modules, and characteristics testing of fiber optic transceiver modules.